RESEARCH　　　　　　　　　　　　　　　　　　　　　　　　　　**Open Access**

Optimized maximum noise fraction for dimensionality reduction of Chinese HJ-1A hyperspectral data

Lianru Gao[1], Bing Zhang[1*], Xu Sun[1], Shanshan Li[1], Qian Du[2] and Changshan Wu[3]

Abstract

The important techniques in processing hyperspectral data acquired by interference imaging spectrometer onboard Small Satellite Constellation for Environment and Disaster mitigation (HJ-1A) are studied in this article. First, a new noise estimation method, named residual-scaled local standard deviations, is used to analyze the noise condition of HJ-1A hyperspectral images. Then, an optimized maximum noise fraction (OMNF) transform is proposed for dimensionality reduction of HJ-1A images, which adopts an accurately estimated noise covariance matrix for noise whitening. The proposed OMNF method is less sensitive to noise distribution and interference existence, thus it can more efficiently compact useful data information in a low-dimensional space. The proposed OMNF is evaluated through two applications, i.e., spectral unmixing and classification, using the HJ-1A image acquired at the Bohai Sea area in China. It demonstrates that the proposed OMNF provides better performance in comparison with other traditional dimensionality reduction methods.

Keywords: Hyperspectral image, Dimensionality reduction, Maximum noise fraction transform, Noise estimation, Classification, Spectral unmixing

1. Introduction

Hyperspectral images contain abundant spatial, spectral, and radiometric information of earth surfaces, which makes earth observation and information acquisition much more effective and efficient for some applications [1,2]. Hyperspectral remote sensing images can be acquired through airborne or spaceborne sensors. There are two remote sensing satellites carrying hyperspectral imagers in China: the moon exploration satellite CE-1 launched during 2007 and the small satellite constellation for environment and disaster mitigation (HJ-1A) launched during 2008. The hyperspectral imager carried on HJ-1A satellite (HJ1A-HSI) is the first spaceborne hyperspectral imager in China, which is also one of few international spaceborne imaging spectrometers [3]. Instead of adopting the traditional dispersion element to acquire spectrometry, this spectrometer employs an advanced interference spectrometry technique. HJ1A-HSI

first acquires an interference curve for each pixel, and then uses the Fourier transform to convert interference curves to spectral curves. The interference spectrometer is modulated across space using the Sagnac interference approach. Its successful operation and application open a new era of Chinese earth observation technology. Although HJ-1A has been operated for several years, new developments for HJ-1A data processing are important for further research and application due to the new interference spectrometry technique used in the sensor.

In general, a hyperspectral image contains hundreds of bands with high spectral resolution, which brings about difficulty in data processing due to data redundancy and complexity. Furthermore, the special characteristic of HJ-1A data (i.e., the distribution of noise and interference present in spectral and spatial domain) makes its application more difficult. Therefore, efficient dimensionality reduction remains as one of the key issues for HJ-1A data processing. Principal component analysis (PCA), which is widely used for dimensionality reduction in hyperspectral image processing [4,5], transforms raw hyperspectral data into a new feature space with

* Correspondence: zhangbing@ceode.ac.cn
[1]Key Laboratory of Digital Earth, Institute of Remote Sensing and Digital Earth, Chinese Academy of Sciences, Beijing 100094, China
Full list of author information is available at the end of the article

mutually orthogonal coordinates. It preserves most information of original data in a low-dimensional space. However, the performance of PCA strongly depends on noise characteristics. When noise variance is larger than signal variance in one band or when the noise is not uniformly distributed between each band, PCA cannot guarantee that image quality decreases for principal components with lower ranking [6]. This drawback limits its application for hyperspectral images, which generally have very different types of noise. For example, in hyperspectral unmixing, noisy pixels might be extracted as endmembers which normally correspond to known and macroscopically pure materials.

Recently, some new approaches have been proposed to deal with noise. One of the most popular ones is the maximum noise fraction (MNF) transform [6,7]. Similar to PCA, MNF also transforms the original data to a feature space; however, features are arranged in terms of image quality, which is measured with signal-to-noise ratio (SNR). In MNF, noise covariance matrix (NCM) needs to be estimated [8-10], which is a key step. In the original MNF, only spatial information is used for NCM estimation, which may not effectively handle special noise with regular pattern, such as interference in HJ-1A data.

There are many methods developed for noise estimation in image analysis [2]. Some traditional approaches use homogeneous area (HA) selection and spatial character analysis, such as HA method [11], Geo-statistical method [11], and local mean and local standard deviation method [12]. However, these methods are easily affected by land cover types in the image. To solve this problem, Roger and Arnold [13] proposed Spectral and Spatial De-Correlation (SSDC) method. Compared with traditional methods, SSDC is more stable, and is widely used. However, SSDC also has some limitations. For example, the noise estimation may be inaccurate when hyperspectral image mainly contains one earth object with absorption feature in some bands, or when the image has a specific complex texture [14]. Residual-scaled Local Standard Deviations method (RLSD) [15] estimates signals according to high spectral correlation and eliminates the influence of complex texture and absorption feature by statistical analysis of sub-blocks. Thus, it is more stable than the SSDC and Homogeneous Regions Division and Spectral De-Correlation method [14], especially for hyperspectral images mainly covered by water. In this article, based on the characteristics of HJ-1A data, we use RLSD for SNR estimation and noise distribution analysis. Then, we propose an optimized MNF (OMNF) transform for dimensionality reduction, which contains two steps: the NCM is calculated via the SSDC, followed by the OMNF transform. Moreover, we propose an assessment framework to evaluate the performance of OMNF via spectral unmixing and classification.

The remainder of this article is organized as follows. Section 2 introduces OMNF method. Section 3 describes experimental image database, performance assessment framework, and comparative analysis methods. In Section 4, noise characteristics of HJ-1A image are analyzed, and evaluation of OMNF using spectral unmixing and classification is presented. Section 5 draws conclusions.

2. OMNF transform

Let $\mathbf{X}$ be a hyperspectral image data, $\mathbf{S}$ and $\mathbf{N}$ are signal component and noise component contained in image data, respectively. Assume $\mathbf{S}$ and $\mathbf{N}$ are uncorrelated, then $\mathbf{X}$ follows a linear model:

$$\mathbf{X} = \mathbf{S} + \mathbf{N} \tag{1}$$

Then, data covariance matrix can be represented as

$$\sum = \sum\nolimits_S + \sum\nolimits_N \tag{2}$$

where $\sum_S$ and $\sum_N$ are the covariance matrix of $\mathbf{S}$ and $\mathbf{N}$, respectively. The MNF transform is expressed as

$$\mathbf{Y} = \mathbf{A}\mathbf{X} \tag{3}$$

where $\mathbf{Y}$ is the MNF result of $\mathbf{X}$, $\mathbf{A}$ is the MNF transform matrix. SNR of each component in $\mathbf{Y}$ can be analyzed as

$$\frac{\mathrm{Var}\{\mathbf{a}_i^{\mathrm{T}}\mathbf{X}\}}{\mathrm{Var}\{\mathbf{a}_i^{\mathrm{T}}\mathbf{N}\}} = \frac{\mathbf{a}_i^{\mathrm{T}}\sum \mathbf{a}_i}{\mathbf{a}_i^{\mathrm{T}}\sum_N \mathbf{a}_i} \tag{4}$$

where Var{} computes the variance, $\mathbf{a}_i$ is the ith component in $\mathbf{A}$. Then we can obtain

$$\sum\nolimits_N^{-1}\sum \mathbf{A} = \Lambda\mathbf{A} \tag{5}$$

where Λ and $\mathbf{A}$ are the eigenvalue matrix and eigenvector matrix of $\sum_N^{-1}\sum$, respectively. MNF is also called noise-adjusted principal components analysis which contains two steps [16,17]. The first step is noise whitening of the hyperspectral image, then PCA is applied to noise whitened data. The main difference between conventional PCA and MNF is that MNF has a prior step of noise whitening, which needs to estimate the NCM. The original MNF method mainly adopts the spatial feature of image to estimate $\sum_N$, such as minimum/maximum autocorrelation factor (MAF), causal simultaneous autoregressive, and quadratic surface [18]. However, as shown in some studies [8-10], space-based noise estimation method is data-selective and unstable. This is because when hyperspectral image has low spatial resolution, the difference between pixels may mainly contain signal. Sometimes, noise with regular pattern, e.g., interference in spatial domain, may be considered as signal when only spatial features are used in noise estimation for MNF.

In hyperspectral images, correlation between bands generally is very large. Therefore, high correlations between bands can also be used for noise estimation, such as SSDC, which is a very useful method for hyperspectral noise estimation [13]. SSDC makes use of the high correlation of hyperspectral data in spatial and spectral domain together, where the radiation value of adjacent bands and pixels is used to estimate the radiation signal value of current pixel through multiple linear regression. Then the estimated radiation signal value is deducted from the actual radiation value of the current pixel, and the remaining value is considered as noise. However, since hyperspectral images do not completely meet the hypothesis adopted in SSDC, we cannot estimate the noise images following model (1). For example, there still is some correlation between noise images. Therefore, implementation of SSDC in Greco et al.'s study [9] is not feasible to estimate NCM for hyperspectral data.

2.1. NCM estimation

The most difference between MNF and OMNF is that OMNF adopts more accurate noise covariance estimation. In the proposed OMNF, noise image computed by SSDC can be used to estimate NCM. In order to control the influence of spatial feature, the image is divided into non-overlapping small sub-blocks, where noise image

**Table 1 Parameters of the HJ-1A IFIS, HYPERION, and CHRIS**

Sensor	IFIS/HJ-1A	HYPERION	CHRIS
Platform attitude (km)	649	705	695
Spectral range (nm)s	450–950	356–2577	400–1019
Average spectral resolution (nm)	5	10	6/33
Time period (days)	4	16	7
Spatial resolution (m)	100	30	17/34
Swath (km)	60	13	7.75
Band number	115	242	18/62

estimated by residual of each sub-block can be used to calculate NCM. SSDC adopted in this article uses multiple linear regression to estimate noise image:
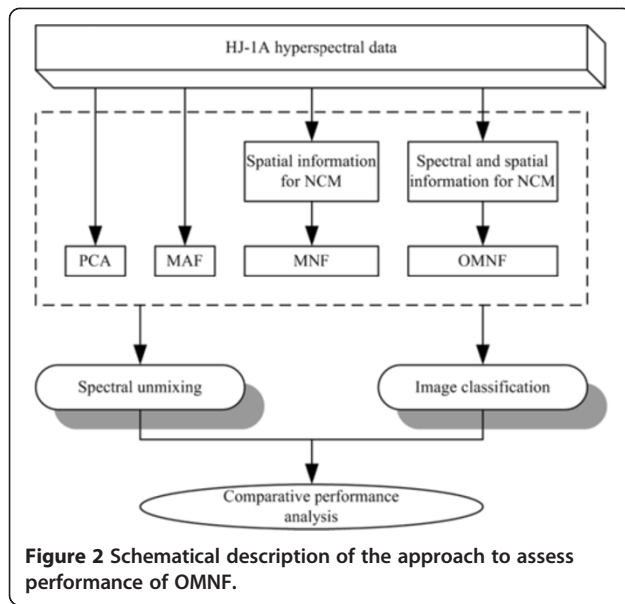
$$x_{i,j,k} = a + bx_{i,j,k-1} + cx_{i,j,k+1} + dx_{p,k} \tag{6}$$

where $x_{i,j,k}$ is the pixel value of band k at (i, j) in a certain sub-block, $x_{i,j,k-1}$ and $x_{i,j,k+1}$ are pixel values in band $k - 1$ and $k + 1$, $x_{p,k}$ is the pixel value spatially near $x_{i,j,k}$ in band k, a, b, c, and d are parameters which need to be estimated through multiple linear regression. In (6), $x_{p,k}$ is defined as

$$x_{p,k} = \begin{cases} x_{i-1,j,k}; & i > 1, \quad j = 1 \\ x_{i,j-1,k}; & j > 1 \end{cases} \tag{7}$$
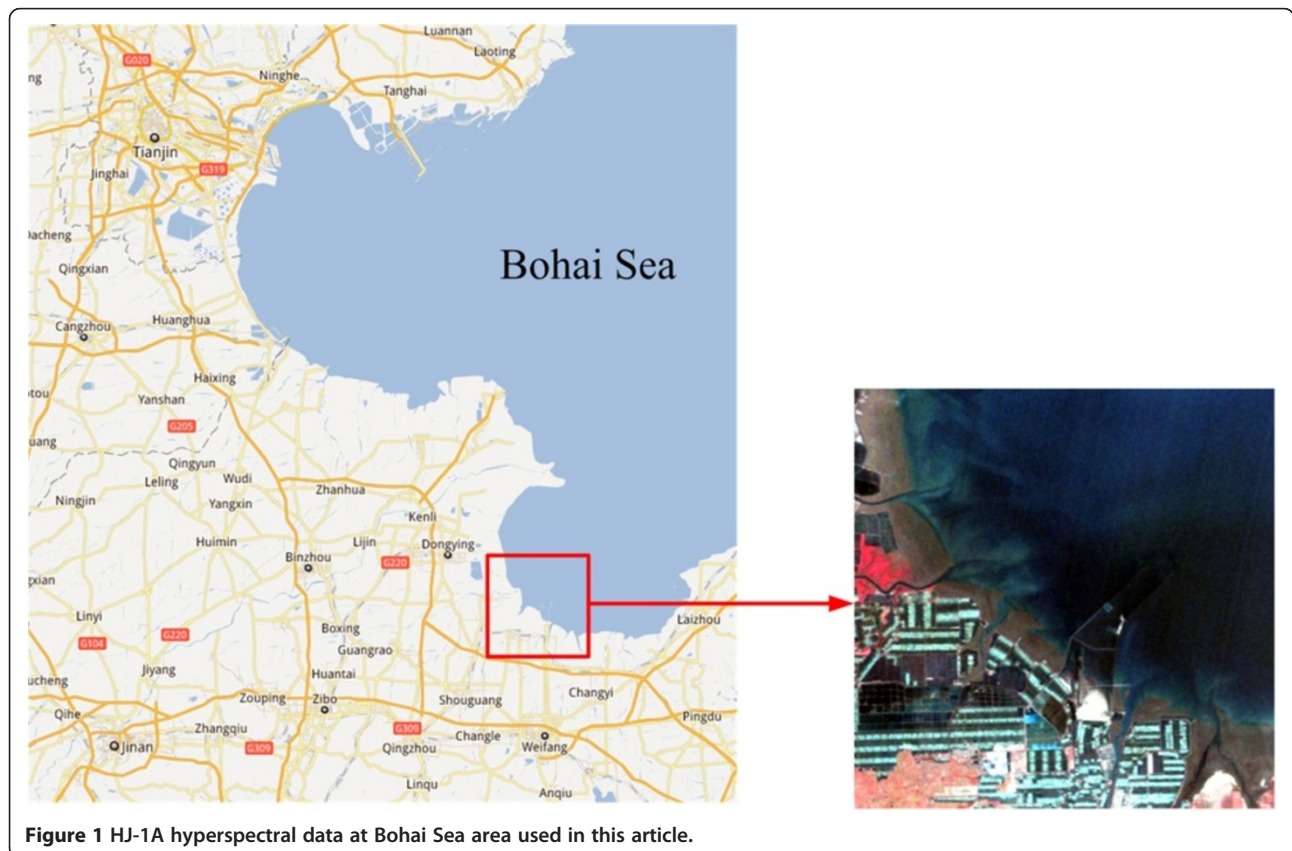
Figure 1 HJ-1A hyperspectral data at Bohai Sea area used in this article.

Figure 2 Schematical description of the approach to assess performance of OMNF.

where the pixel located at (1,1) of the sub-block is not considered. SSDC estimates possible signal value $\hat{x}_{i,j,k}$ at band k from the obtained parameters. Then, noise of each pixel can be obtained through $r_{i,j,k} = x_{i,j,k} - \hat{x}_{i,j,k}$. Finally, the NCM for OMNF can be calculated as follows:

$$
\begin{aligned}
\sigma_k^2 &= \sum_{i=1}^{H} \sum_{j=1}^{W} \left(r_{i,j,k} - \bar{r}_{i,j,k} \right)^2, C_{kl} \\
&= \sum_{i=1}^{H} \sum_{j=1}^{W} \left(r_{i,j,k} - \bar{r}_{i,j,k} \right) \left(r_{i,j,l} - \bar{r}_{i,j,l} \right), \quad 1 \le k, \quad l \le N
\end{aligned}
\tag{8}
$$

where $(i,j) \neq (1,1)$, W, H are the width and height of image, respectively, and N is the total number of bands.

2.2. OMNF transformation
After noise variance is estimated through (8), noise correlation is removed through noise whitening with

(5). Finally, dimensionality reduction can be performed through (3).

3. Experiments design and assessment methods
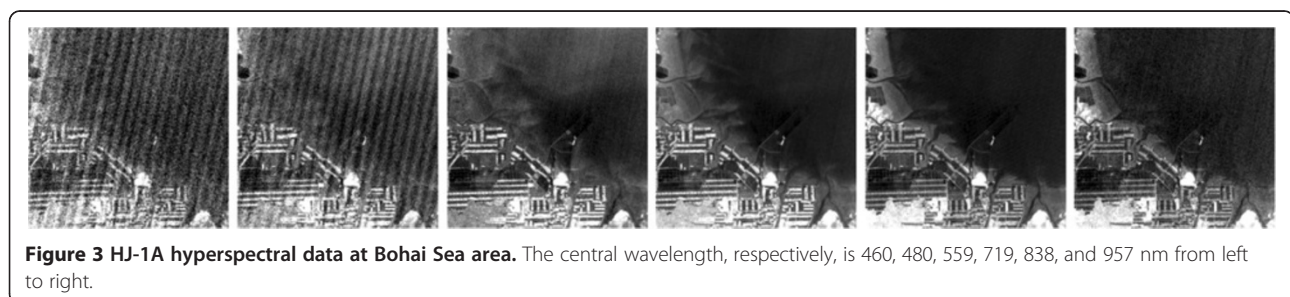### 3.1. HJ-1A hyperspectral data
The InterFerometric Imaging Spectrometer (IFIS) installed on HJ-1A is the first hyperspectral earth observation sensor in China [3]. Its spectrum ranges from 0.45 to 0.95 μm with 115 spectral bands. The average spectral resolution is about 5 nm. The nominal ground sample distance is 100 m with an image swath of about 60 km. IFIS is a typical Sagnac imaging Fourier transform spectrometer featured by a compact structure, small volume, and light weight. Table 1 lists the parameters of the IFIS on HJ-1A comparing to those of HYPERION on Earth Observing 1 (EO-1) and Compact High Resolution Imaging Spectrometer (CHRIS) on PRoject for On-Board Autonomy (PROBA). This hyperspectral imaging sensor has excellent specifications for practical applications. However, the data quality is degraded by severe noise. The new interferometric spectrometer technique is used in this sensor, which makes that the noise characteristics of IFIS are very different from noise contained in normal dispersion spectrometry used in HYPERION and CHRIS. For instance, regular striping noise is still present after calibration, and cannot effectively be removed by Fourier transform and notch filter method. Therefore, effective noise removal is crucial.

In this article, HJ-1A images at Bohai Sea area are chosen for experiments (Figure 1). The HJ-1A hyperspectral images used here contain 115 bands, and 400 × 400 pixels.
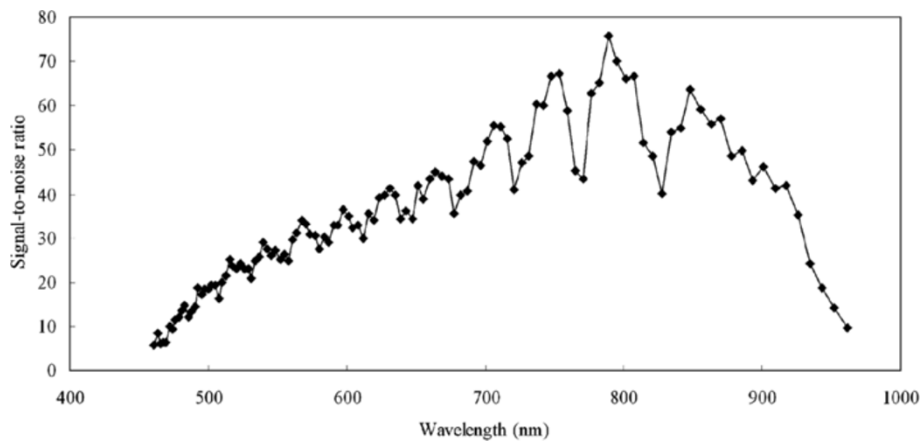
3.2. Noise characteristics analysis
Image noise may be periodic noise or random noise. Periodic noise can effectively be eliminated through frequency domain filtering, such as notch or bandpass filtering. However, it is more complex to effectively remove random noise, which is generally assumed to be additive Gaussian white noise [19,20]. In this article, we propose to use RLSD [15] for noise estimation. In summary, RLSD procedure is described as follows:
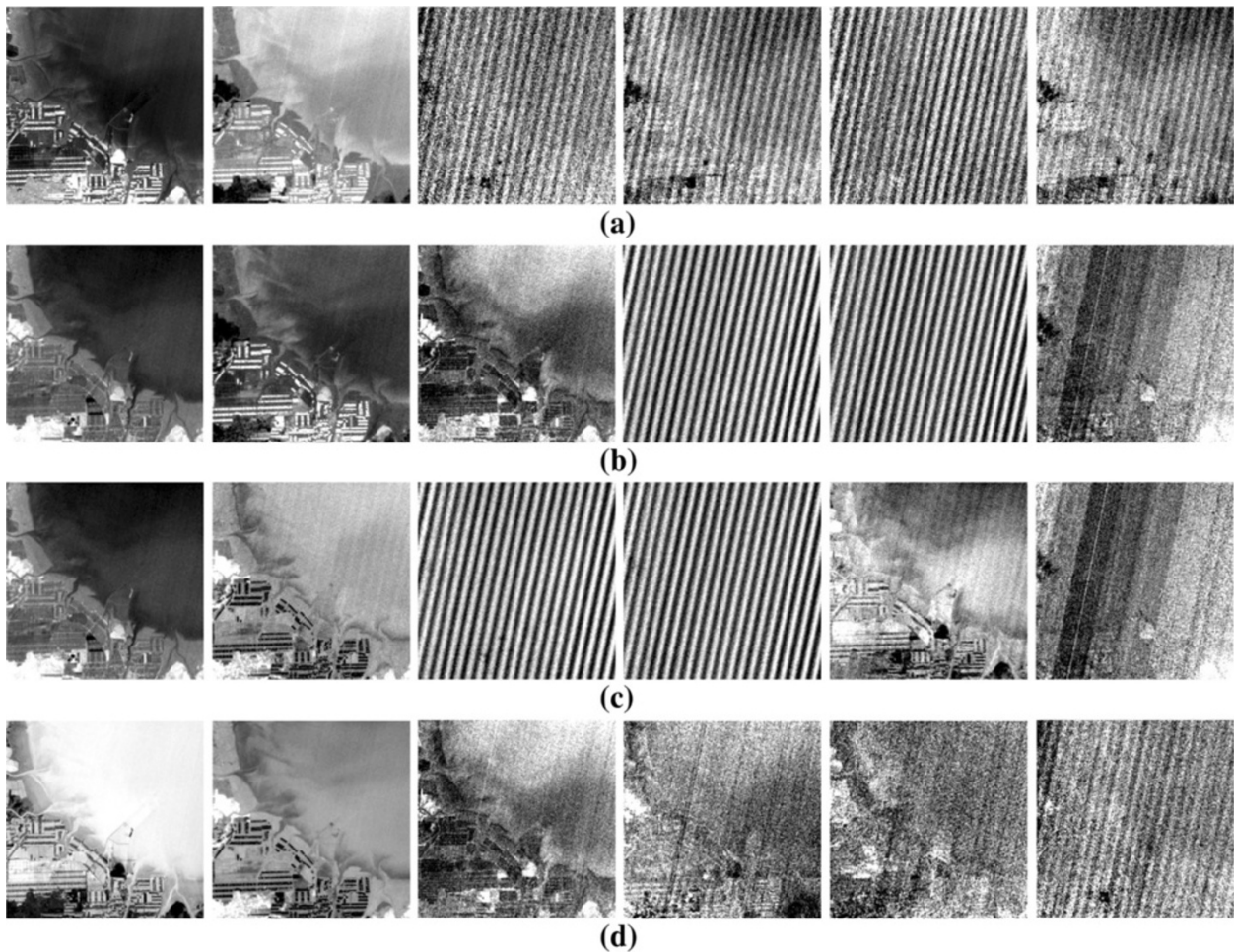
Step 1: We divide the image into many small rectangular sub-blocks, and then calculate parameters a, b, and


Figure 3 HJ-1A hyperspectral data at Bohai Sea area. The central wavelength, respectively, is 460, 480, 559, 719, 838, and 957 nm from left to right.

Figure 4 SNR estimation results of HJ-1A hyperspectral data at Bohai Sea area.

Figure 5 Results of dimensionality reduction through PCA (a), MAF (b), traditional MNF (c), and OMNF (d). In each row, the image from first to sixth components in transformed data is represented from left to right.
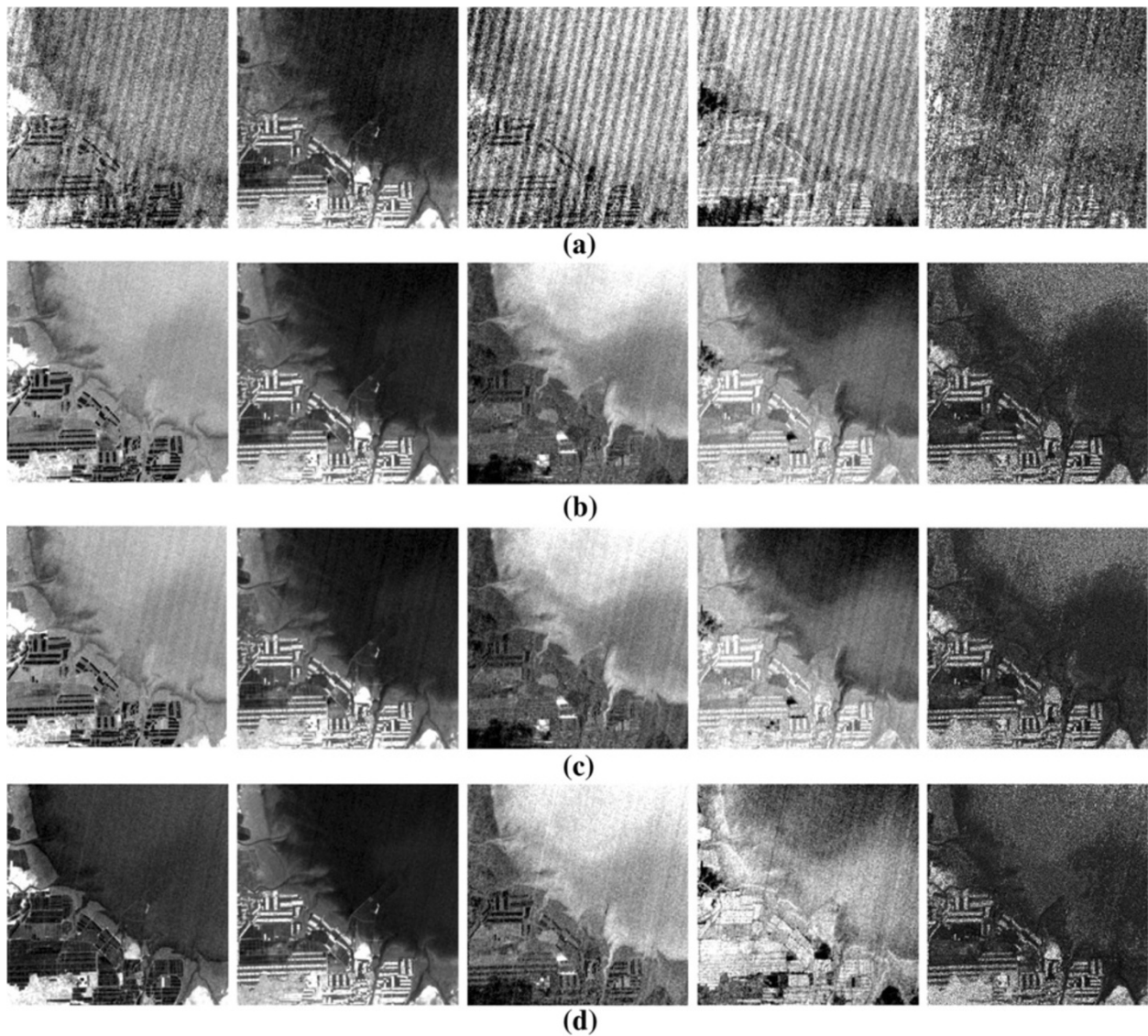
Figure 6 Abundance estimation results of extracted endmembers by N-FINDR. Abundance retrieval is processed based on dimensionality reduced HJ-1A hyperspectral data through PCA (**a**), MAF (**b**), traditional MNF (**c**), and OMNF (**d**). In each row, vegetation, salt area, muddy water, water body, and error are represented from left to right.

c of signal component in each sub-block through multiple linear regression:

$$\mathbf{x}_k = a + b\mathbf{x}_{k-1} + c\mathbf{x}_{k+1} \qquad (9)$$

Here, $\mathbf{x}_k$ is a vector with $N \times 1$ values, where $N = w \times h$ with w and h being width and height of a certain sub-block at band k, respectively. Then, the estimated signal value $\hat{\mathbf{x}}_k$ is calculated through the obtained parameters and pixel value at adjacent bands. Finally, the residuals are obtained by: $\mathbf{r} = \mathbf{x}_k - \hat{\mathbf{x}}_k$. Since the predictable signal information between bands is removed, the remained 'unexplained' residuals can approximate noise.

Step 2: The Local Standard Deviation (LSD) is calculated at each sub-block as follows:

$$LSD = \left[(M-3)^{-1}S^2\right]^{1/2} \qquad (10)$$

where M is the number of pixels of this sub-block and S^2 is the variance of residuals of the sub-block. As there are three parameters used in multiple linear regression shown in (9), the unbiased estimation requires the term of $M - 3$.

Step 3: After LSDs of all sub-blocks are calculated, we extract maximum and minimum values of the obtained LSDs. Then, several bins with equal

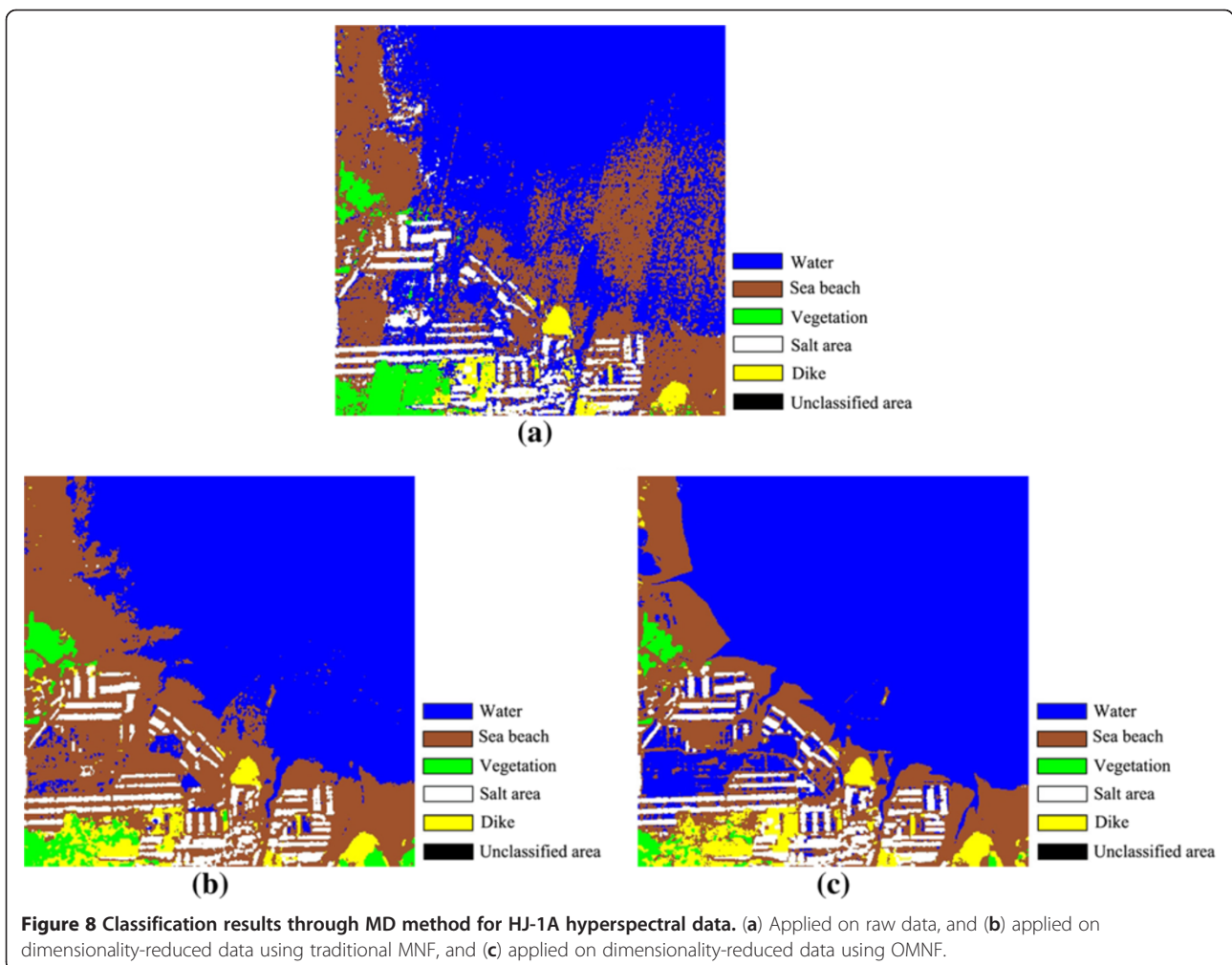**Figure 7 Training and testing samples used in classification experiments.**
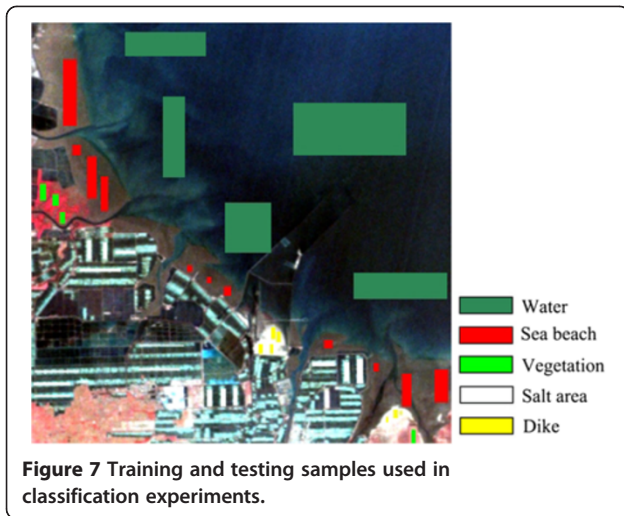
interval are set between these two values. The numbers of sub-blocks in each bin can be counted according to its LSD value. Finally, the mean LSD value of the bin with the most number of blocks is calculated, which can be considered as the noise of the whole image.
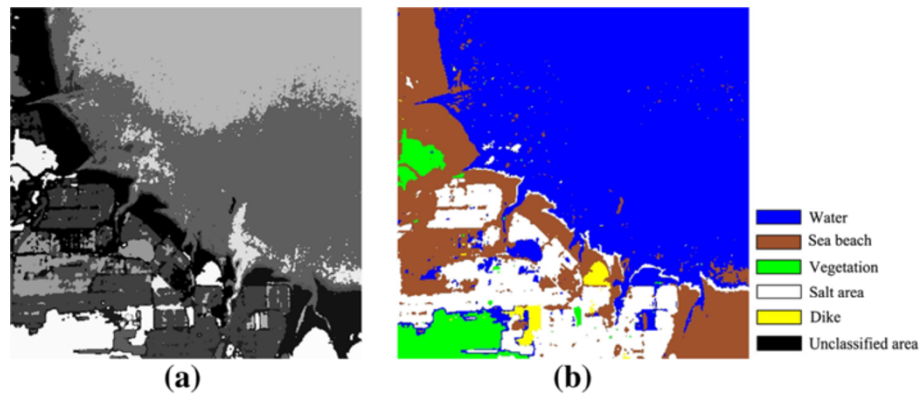
3.3. Assessment framework and methods

We consider several dimensionality reduction methods, i.e., PCA, MAF, MNF, and OMNF, for evaluation. Since the spatial resolution of HJ-1A hyperspectral data is 100 m, mixed pixels generally exist in the image. Therefore, we consider spectral unmixing for evaluation from full-pixel scale to sub-pixel scale. Similarly, image classification is also considered for evaluation as it has important applications. Figure 2 shows the flowchart of the proposed scheme.

3.3.1. Spectral unmixing method

Spectral unmixing mainly obtains endmember extraction and abundance estimation [21,22]. Endmember extraction

Figure 8 Classification results through MD method for HJ-1A hyperspectral data. (**a**) Applied on raw data, and (**b**) applied on dimensionality-reduced data using traditional MNF, and (**c**) applied on dimensionality-reduced data using OMNF.

Figure 9 Classification result through MNF and HOE for HJ-1A hyperspectral data. (**a**) The result of image segmentation, and (**b**) the result of image classification.

extracts pure pixels. Abundance estimation estimates the proportion of each endmember in a mixed pixel. In spectral unmixing, abundance estimation generally adopts a least squares method (constrained or unconstrained). Many endmember extraction methods are developed, such as, Pixel Purity Index (PPI), N-FINDR, Vertex Component Analysis (VCA), Iterative Error Analysis (IEA), and so on [22].

In the aforementioned methods, N-FINDR is one of the most widely used algorithms [23]. Its aim is to find a set of pixels that can construct a simplex with the maximum volume. These pixels can be considered as endmembers. Due to the requirement of a square matrix used in volume calculation in N-FINDR, the original image must be transformed to a $(p - 1)$-dimensional subspace by a dimensionality reduction method.

3.3.2. Image classification method

Hyperspectral classification can be supervised or unsupervised, parametric or non-parametric, and hard or soft (fuzzy). Traditional pixel-based classification methods, such as Maximum Likelihood Classifier (MLC), Spectral Angle

Mapper (SAM), Minimum Distance Classifier (MDC), analyze data without incorporating spatial information. However, spatial information can play an important role in hyperspectral image classification [24]. Classification accuracy can greatly be improved when spatial and spectral features are effectively combined [25]. In this study, we propose to use a Homogenous Objects Extraction (HOE)-based method to combine spectral and spatial information for classification. Meanwhile, the HOE method can efficiently deal with the special noise present in HJ-1A data.

In homogenous object-oriented image classification, such as HOE, the key issue is to extract the objects with high homogeneity. Non-uniform radiation response increases spectral variation, which is common with the high degree of spectral heterogeneity in complex landscape. Thus, in the HOE-based classification approach used in this study, all pixels inside a homogeneous object can be considered belonging to the same class. Furthermore, since homogeneous regions are extracted through spectral similarity between pixel and neighborhoods, integration of spectral feature and a series of
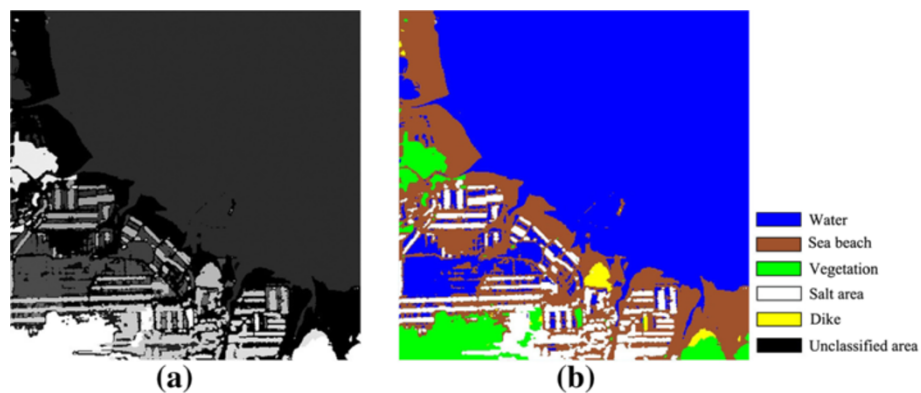
Figure 10 Classification result through OMNF and HOE for HJ-1A hyperspectral data. (**a**) The result of image segmentation, and (**b**) the result of image classification.
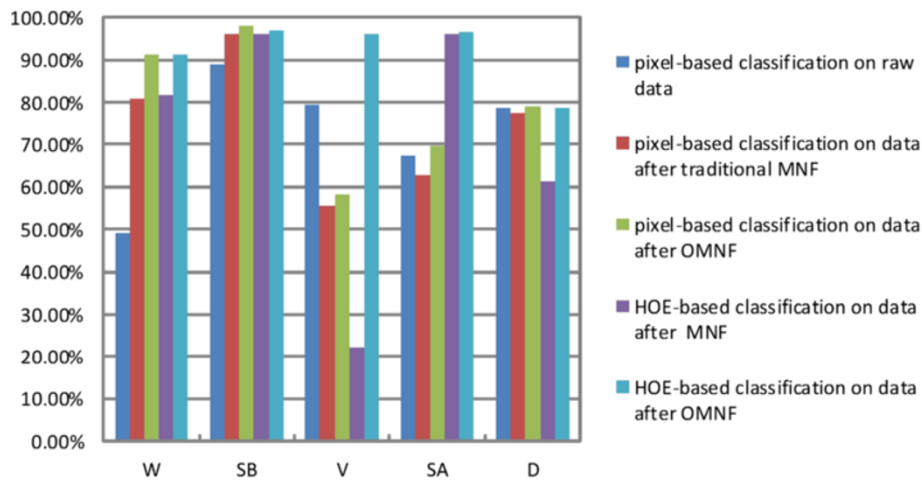
Figure 11 Producer's accuracy comparison of pixel-based classification and HOE-based classification, where classified earth objects are water (W), sea beach (SB), vegetation (V), salt area (SA), and dike (D).

spatial features (such as shape, size, texture, and context relationship) can be applied in classification. This approach mainly includes three steps: image segmentation, feature extraction, and classification.

Image segmentation
In this article, fuzzy K-means clustering is used for image segmentation. Fuzzy K-means is a soft clustering algorithm which determines the subordination degree of each pixel in each type according to that of its vector value between [0, 1]. This algorithm is an iterative process, where each type of centroids (c_i) and pixel subordination matrix (u_{ij}) are adjusted using (11) until

the convergence of objection function $J = \sum_{i=1}^{k} \sum_{j=1}^{n} u_{ij}^m d_{ij}^2$.

$$c_i = \frac{\sum_{j=1}^{n} u_{ij}^m x_j}{\sum_{j=1}^{n} u_{ij}^m}, \quad \text{where } u_{ij}$$

$$= \left[\sum_{k=1}^{c} \left(\frac{d_{ij}}{d_{kj}} \right)^{2/(m-1)} \right]^{-1}, \tag{11}$$

where $m \in [1, \infty]$ is a weighted index, d_{ij} is dissimilarity measurement, such as Euclidean distance.
Feature extraction
After image segmentation, the features of homogeneous objects can be extracted, which may include the spatial position, spectra of the homogenous object, and its class label. Since all the pixels in the same segment belong to the same class, the class label of the segment can be obtained by tracking the margin through a contour-based object tracking method.

Moreover, the mean spectrum of all pixels in each homogeneous object is used as the spectral feature for this object.
Classification
In general, traditional pixel-based method performs classification by comparing the spectral similarity of each pixel with prior knowledge of the training samples. In the HOE-based method, pixel-wise training samples need to be transformed to objects according to the relationship between a given pixel and its corresponding homogenous object. Such classification model parameters can be estimated by training the objects at different homogeneous regions. As shown in (12), the Mahalanobis Distance (MD) is considered:

$$D(x_i, z_l) = (x_i - z_l)^T \sum_l{}^{-1} (x_i - z_l), \tag{12}$$

where z_l and $\sum_l$ are the mean vector and covariance matrix of training samples, respectively.

4. Experiments and results analysis
4.1. Noise characteristics analysis of HJ-1A hyperspectral data
The diagnostic spectral features of earth materials are required for image classification and information extraction of hyperspectral images. However, hyperspectral sensor acquires data with very small spectral interval. Thus, there is insufficient optical energy for each band. It is much more difficult to improve SNR of hyperspectral data than panchromatic or multispectral images. Absorption feature of the spectrum can be detected only when spectral absorption depth is one magnitude greater than the noise level [26]. During data acquisition, the spectral feature of earth object, however, is easily distorted by noise.

In this study, the size of each sub-block is 8 × 8 pixels. In order to handle the interval bin division (see step 3 in the RLSD procedure), we estimate the noise based on the parameters estimated by the technique proposed in [12], where the bins are set in the range between the minimum LSD and 1.2 times of LSD mean value, and 150 bins are recommended.

Figure 3 illustrates some bands of the considered HJ-1A data at Bohai Sea area. It is noticeable that image quality of these bands is significantly different. This is reasonable, since, according to the interference device used in HJ-1A sensor, spectral information is acquired in a way different from the dispersive spectrometer. It receives interference data modulated and interfered by target spectral information. The ordinary data with spectral radiation information can be obtained through spectral restoration. For the errors produced by interference device and spectral restoration, HJ-1A hyperspectral data are disturbed with periodical strip at spatial domain, which is difficult to be eliminated by traditional radiance calibration methods [3]. Therefore, in order to guarantee the precision and accuracy of image classification and spectral unmixing, this special noise requires specific method to remove.

Figure 4 shows the SNR estimates from RLSD. It can be observed that noise distribution is non-uniform. Furthermore, it is well known that noise condition is more realistic when the image mainly covers water area [27]. Therefore, dimensionality reduction with effective noise-elimination is important for real applications.

4.2. Dimensionality reduction results

Figure 5 shows the six components of the considered dimensionality reduction methods. It can be seen that the first two components obtained from PCA (see Figure 5a) have most information of the data. However, it is possible that these principle components contain noise which is non-uniformly distributed in the spectral domain. Therefore, PCA is not well suitable for dimensionality reduction of HJ-1A data. Furthermore, as shown in Figure 5b, the first three components of MAF have most spatial correlations of the image, which means those components have most volume of the signal. The fourth and fifth components are almost noise. However, the sixth component contains information. This brings difficulty for determining the number of components. Therefore, MAF is also not suitable for dimensionality reduction of HJ-1A hyperspectral images. Moreover, Figure 5c shows the components obtained from MNF. It can be seen that the first two components also have the highest image quality. However, the fifth component contains more information than the third and fourth components, which are interfered by periodic strips. Thus, although traditional MNF takes noise into account and can solve the influence of

non-uniform noise distribution in spectral domain, it is easily affected by the hybrid distributions of earth objects and periodic interference; thus, its components may not be arranged in descending order of image quality. Finally, Figure 5d shows the components obtained by the proposed OMNF method. It can be observed that OMNF reduces data dimensionality more effectively where all components are arranged in descending order of image quality.

4.3. Comparative performance analysis

In this section, the first three components of PCA, MAF, and OMNF are used for spectral unmixing and image classification, and the first, second, and fifth components of traditional MNF are used for spectral unmixing and image classification.

4.3.1. Spectral unmixing

Endmember extraction and abundance estimation by N-FINDR and unconstrained least squares methods are applied to the dimensionality-reduced data obtained from PCA, MAF, MNF, and OMNF. Based on the obtained components, only four endmembers are extracted, and Figure 6 shows the obtained abundance and error maps. Several conclusions can be obtained from Figure 6. First of all, the results obtained from the PCA components are only the salt area is appropriate and all the other endmembers are greatly affected by noise. Furthermore, it can be seen that the results obtained from MAF, MNF, and OMNF components are better than those of PCA, where OMNF obtains the best results. This is because all these methods take noise into account. Moreover, it can be observed that the abundance estimations of vegetation, salt area, muddy water, and water body are more reasonable in geographical distribution than results from other dimensionality reduction methods. This is because OMNF eliminates noise during the dimensionality reduction procedure. For example, distribution of vegetation in abundance map of OMNF is better than others. Another example is distribution of salt area is repeated in the abundance maps of salt area and water body in both MAF and MNF results.

4.3.2. Image classification

Figure 7 shows the reference data on the false color composite. In the dataset, 20% of samples are used for training, and the rest for testing. Training and testing samples were randomly selected from the reference data.

Figure 8 shows the classification results obtained from the raw data, the dimensionality-reduced data from the MNF and OMNF, respectively. It can be seen that the pixel-based classification using OMNF features obtained the best result, especially for the water and sea beach classes.

Figures 9 and 10 illustrate the classification results obtained from the MNF and OMNF features by the HOE method, respectively. Figures 9a and 10a present the segmentation of the hyperspectral image. Two steps are involved in this process. The first step is the fuzzy *K*-means clustering, followed by edge tracking to obtain the boundaries of the ground objects in the second step. As can be seen from Figures 9b and 10b, the classification results are better than those in Figure 8. Overall, classification result using OMNF and HOE is the best.

The producer's accuracy is used for further assessment [28]. Figure 11 shows the classification accuracies, where five methods are considered: pixel-based classification on the raw data, pixel-based classification on reduced data from MNF, pixel-based classification on reduced data from OMNF, HOE-based classification on reduced data from MNF, and HOE-based classification on reduced data from OMNF. It can be observed that HOE-based classification is better than the pixel-based method for water body in most parts of the study area (including water in sea water and salt area in saltern) and for sea beach, vegetation, and salt area in saltern. The obtained Kappa coefficients are 0.4076, 0.6229, 0.6740, 0.7011, and 0.8704 for pixel-based classification on the raw data, pixel-based classification of the MNF-reduced data, pixel-based classification of the OMNF-reduced data, HOE-based classification of the MNF-reduced data, and HOE-based classification of the OMNF-reduced data, respectively. It can be seen that the proposed HOE with OMNF method leads to excellent classification performance, which produced the highest accuracy for the considered HJ-1A hyperspectral image.

5. Conclusion and discussion

Hyperspectral imager carried on HJ-1A satellite indicates a new development stage of hyperspectral remote sensing technology in China. However, due to the new interference spectrometry technique implemented in this sensor, noise characteristics of HJ-1A images are more complex than images acquired by other hyperspectral sensors, such as HYPERION and CHRIS. This article presents an OMNF method for dimensionality reduction for HJ-1A images, which estimates the NCM using SSDC method. The proposed approach is evaluated by a real HJ-1A hyperspectral data at Bohai Sea. Both unmixing and classification results indicate that the proposed method can offer excellent performance for HJ-1A data applications.

Abbreviations

HJ-1A: Small satellite constellation for environment and disaster mitigation; HOE: Homogenous objects extraction-based method; IFIS: Interferometric imaging spectrometer; LSD: Local standard deviation; MAF: Minimum/maximum autocorrelation factor; MD: Mahalanobis distance; MNF: Maximum noise fraction; NCM: Noise covariance matrix; OMNF: Optimized maximum noise fraction transformation; PCA: Principal component analysis; RLSD: Residual-scaled local standard deviations method; SNR: Signal-to-noise ratio; SSDC: Spectral and spatial de-correlation method.

Author details
[1]Key Laboratory of Digital Earth, Institute of Remote Sensing and Digital Earth, Chinese Academy of Sciences, Beijing 100094, China. [2]Department of Electrical and Computer Engineering, Mississippi State University, Mississippi State, MS 39762, USA. [3]Department of Geography, University of Wisconsin-Milwaukee, Milwaukee WI 53201, USA.

References
1. AFH Goetz, G Vane, EJ Solomon, BN Rock, Imaging spectrometry for earth remote sensing. Science 228(4704), 1147–1153 (1985)
2. FD Van Der Meer, SM Dejong, *Imaging Spectrometry: Based Principles and Prospective Applications* (Kluwer Academic Publishers, Netherlands, 2001)
3. B Zhang, Z Chen, J Li, L Gao, Image quality evaluation on Chinese first earth observation hyperspectral satellite, in *International Geoscience and Remote Sensing Symposium*, ed. by, 1st edn. (, Cape Town, South Africa, 2009), pp. I-188–I-191
4. CM Bachmann, TF Donato, GM Lamela, WJ Rhea, MH Bettenhausen, RA Fusina, KRD Bois, JH Porter, BR Truitt, Automatic classification of land cover on smith island, VA, using HyMAP imagery. IEEE Trans. Geosci. Remote Sens. 40(10), 2313–2330 (2002)
5. X Miao, P Gong, S Swope, P Ruiliang, R Carruthers, GL Anderson, JS Heaton, CR Tracy, Estimation of yellow starthistle abundance through CASI-2 hyperspectral imagery using linear spectral mixture models. Remote Sens. Environ. 101(3), 329–341 (2006)
6. AA Green, M Berman, P Switzer, MD Craig, A transformation for ordering multispectral data in terms of image quality with implications for noise removal. IEEE Trans. Geosci. Remote Sens. 26(1), 65–74 (1988)
7. C Gordon, A generalization of the maximum noise fraction transform. IEEE Trans. Geosci. Remote Sens. 38(1), 608–610 (2000)
8. RE Roger, Principal components transform with simple, automatic noise adjustment. Int. J. Remote Sens. 17(14), 2719–2727 (1996)
9. M Greco, M Diani, G Corsini, Analysis of the classification accuracy of a new MNF based feature extraction algorithm, in *Proceedings of SPIE*, ed. by, 6365th edn. (, Stockholm, Sweden, 2006), p. 63650V
10. X Liu, B Zhang, L Gao, D Chen, A maximum noise fraction transform with improved noise estimation for hyperspectral data. Sci. Chin. Ser. F-Inf. Sci. 52(9), 1578–1587 (2009)
11. PJ Curran, JL Dungan, Estimation of signal-to-noise: a new procedure applied to AVIRIS data. IEEE Trans. Geosci. Remote Sens. 27(5), 620–628 (1989)
12. B-C Gao, An operational method for estimating signal to noise ratios from data acquired with imaging spectrometers. Remote Sens. Environ. 43(1), 23–33 (1993)
13. RE Roger, JF Arnold, Reliably estimating the noise in AVIRIS hyperspectral data. Int. J. Remote Sens. 17(10), 1951–1962 (1996)
14. L Gao, B Zhang, X Zhang, W Zhang, Q Tong, A new operational method for estimating noise in hyperspectral datas. IEEE Geosci. Remote Sens. Lett. 5(1), 83–87 (2008)
15. L Gao, B Zhang, J Wen, Q Ran, A residual-scaled local standard deviations method for estimating noise in hyperspectral data, in *Proceedings of SPIE*, ed. by H Maître, H Sun, J Liu, E Song, 6787th edn. (, Wuhan, China, 2007), p. 678713
16. JB Lee, AS Woodyatt, M Berman, Enhancement of high spectral resolution remote-sensing data by a noise-adjusted principal components transform. IEEE Trans. Geosci. Remote Sens. 28(3), 295–304 (1990)

17. RE Roger, A faster way to computer the noise-adjusted principal components transform matrix. IEEE Trans. Geosci. Remote Sens. **32**(6), 1194–1196 (1994)
18. AA Nielsen, *Analysis of regularly and irregularly sampled spatial, multivariate and multi-temporal data* (Dissertation, Technical University of Denmark, 1994)
19. Q Du, Noise estimation for remote sensing image data analysis, in *Proceedings of SPIE*, ed. by SS Shen, PE Lewis (, Bellingham, WA, 2003)
20. BR Corner, RM Narayanan, SE Reichenbach, Noise estimation in remote sensing imagery using data masking. Int. J. Remote Sens. **24**(4), 689–702 (2003)
21. N Keshava, JF Mustard, Spectral unmixing. IEEE Signal Process. Mag. **19**(1), 44–57 (2002)
22. A Plaza, P Martínez, R Pérez, J Plaza, A quantitative and comparative analysis of endmember extraction algorithms from hyperspectral data. IEEE Trans. Geosci. Remote Sens. **42**(3), 650–663 (2004)
23. ME Winter, N-FINDR: an algorithm for fast autonomous spectral end-member determination in hyperspectral data, in *Proceedings of SPIE*, ed. by MR Descour, SS Shen, 3753rd edn. (, Denver, USA, 1999), pp. 266–275
24. A Plaza, JA Benediktsson, J Boardman, J Brazile, L Bruzzone, G Camps-Valls, J Chanussot, M Fauvel, P Gamba, JA Gualtieri, M Marconcini, JC Tilton, G Trianni, Recent advances in techniques for hyperspectral image processing. Remote Sens. Environ. **113**(Suppl1), S110–S122 (2009)
25. LO Jiménez, JL Rivera-Medina, E Rodríguez-Díaz, E Arzuaga-Cruz, M Ramírez-Vélez, Integration of spatial and spectral information by means of unsupervised extraction and classification for homogenous objects applied to multispectral and hyperspectral data. IEEE Trans. Geosci. Remote Sens. **43**(4), 844–851 (2005)
26. FH Goetz, WM Calvin, Imaging spectrometry: spectral resolution and analytical identification of spectral features, in *Imaging Spectroscopy II; Proceedings of the Meeting 0834*, ed. by (, San Diego, CA, 1987), pp. 158–165
27. L Gao, Q Du, W Yang, B Zhang, A comparative study on noise estimation for hyperspectral imagery, in *IEEE 4th Workshop on Hyperspectral Image and Signal Processing: Evolution in Remote Sensing (WHISPERS'12)*, ed. by (, Shanghai, China, 2012)
28. RG Congalton, A review of assessing the accuracy of classifications of remotely sensed data. Remote Sens. Environ. **37**(1), 35–46 (1991)